

Cortical functional connectivity across the adult lifespan and its relation to sensorimotor integration

Santeri Ruuskanen^{a,*}, Juan Camilo Avendano-Diaz^a, Mia Liljeström^{a,b}, and Lauri Parkkonen^a

^aDepartment of Neuroscience and Biomedical Engineering, Aalto University, Espoo, Finland

^bBioMag Laboratory, HUS Medical Imaging Center, Helsinki University Hospital, Helsinki, Finland

*Corresponding author: Santeri Ruuskanen, santeri.ruuskanen@aalto.fi

Abstract

The operation of the human brain relies on functional networks enabled by inter-areal oscillatory synchronization between neuronal populations. Although disruptions in this functional connectivity are associated with brain disorders, evidence on its healthy age-dependent variation and behavioral relevance remains limited. Utilizing magnetoencephalography (MEG) recordings from 576 adults, we investigated the evolution of resting-state functional connectivity (rs-FC) across the healthy adult lifespan. We observed age-related, frequency-specific changes in widespread cortical networks. Alpha-band (8–13 Hz) rs-FC decreased and theta-band (4–8 Hz) rs-FC increased with age, while beta-band (13–30 Hz) rs-FC followed a non-linear trajectory, peaking in middle age. These patterns differed from concurrent changes in oscillatory power, underscoring their dissociable contributions. Notably, reduced beta-band rs-FC was associated with increased sensorimotor attenuation, indicating that changes in rs-FC are behaviorally relevant. These findings advance our understanding of healthy brain aging and highlight a link between resting-state brain activity and sensorimotor integration.

Keywords: aging — lifespan — functional connectivity — brain oscillations — magnetoencephalography — resting-state — sensorimotor attenuation

Main

The aging human brain undergoes widespread structural and functional changes which are accentuated in various neuropathologies [1–10]. It is now well established, based on magnetic resonance imaging (MRI), that cortical thickness and gray matter volume decrease throughout the adult lifespan [1]. Moreover, diffusion-weighted MRI and functional MRI (fMRI) studies have revealed age-related trends in structural and functional brain networks [2–4]. In addition, evidence from non-invasive electrophysiological techniques including electroencephalography (EEG) and magnetoencephalography (MEG) suggests that spontaneous neuronal oscillations possess unique frequency-dependent trajectories across the lifespan [5, 10]. However, research on age-related trends in the inter-areal functional coupling between these spontaneous oscillations, referred to as resting-state functional connectivity (rs-FC), and their behavioral relevance remains limited. Nevertheless, functional connectivity between brain areas is vital for normal brain function and disrupted in neuropathological conditions typically associated with aging, such as Parkinson’s and Alzheimer’s disease [6–9, 11]. Accurately characterizing the healthy variability in rs-FC is essential to distinguish normal aging from pathological deviations and to optimally utilize rs-FC as a potential disease biomarker.

Changes in MEG rs-FC related to healthy aging have been sparsely investigated, and the findings remain inconclusive. An early study reported age-related increases in directed rs-FC into the medial temporal lobe and decreased rs-FC into the posterior cingulum and precuneus across broad frequency ranges within 1–100 Hz [12]. Others have reported decreased sensor-level global coherence in the alpha frequency band across the lifespan [13] and increased variability of the phase-locking value (PLV) within the default mode network (DMN) in the delta frequency band in older adults [14]. In contrast, a more recent study found no significant age-related changes in the imaginary part of coherency (ImC) in the delta band, and reported increased connectivity of posterior, parietal, and temporal regions in the theta and gamma bands, as well as decreased alpha and beta connectivity with age in temporal and posterior areas, respectively [15]. Another recent report suggested more complex patterns of generally decreasing connectivity in the delta band, nonlinear trends in the theta and alpha bands, and increasing connectivity in the beta and gamma bands [16]. Notably, in contrast to these studies utilizing connectivity metrics based on phase synchronization, Coquelet and colleagues [17] did not observe any significant age-related changes in connectivity using power envelope correlations.

Despite common elements across the findings of previous studies, research in the area has not yet converged. This incongruity could be largely attributed to methodological differences between studies. Besides limited sample sizes, we identified four main methodological considerations that could confound rs-FC studies. First, a major challenge in electrophysiological functional

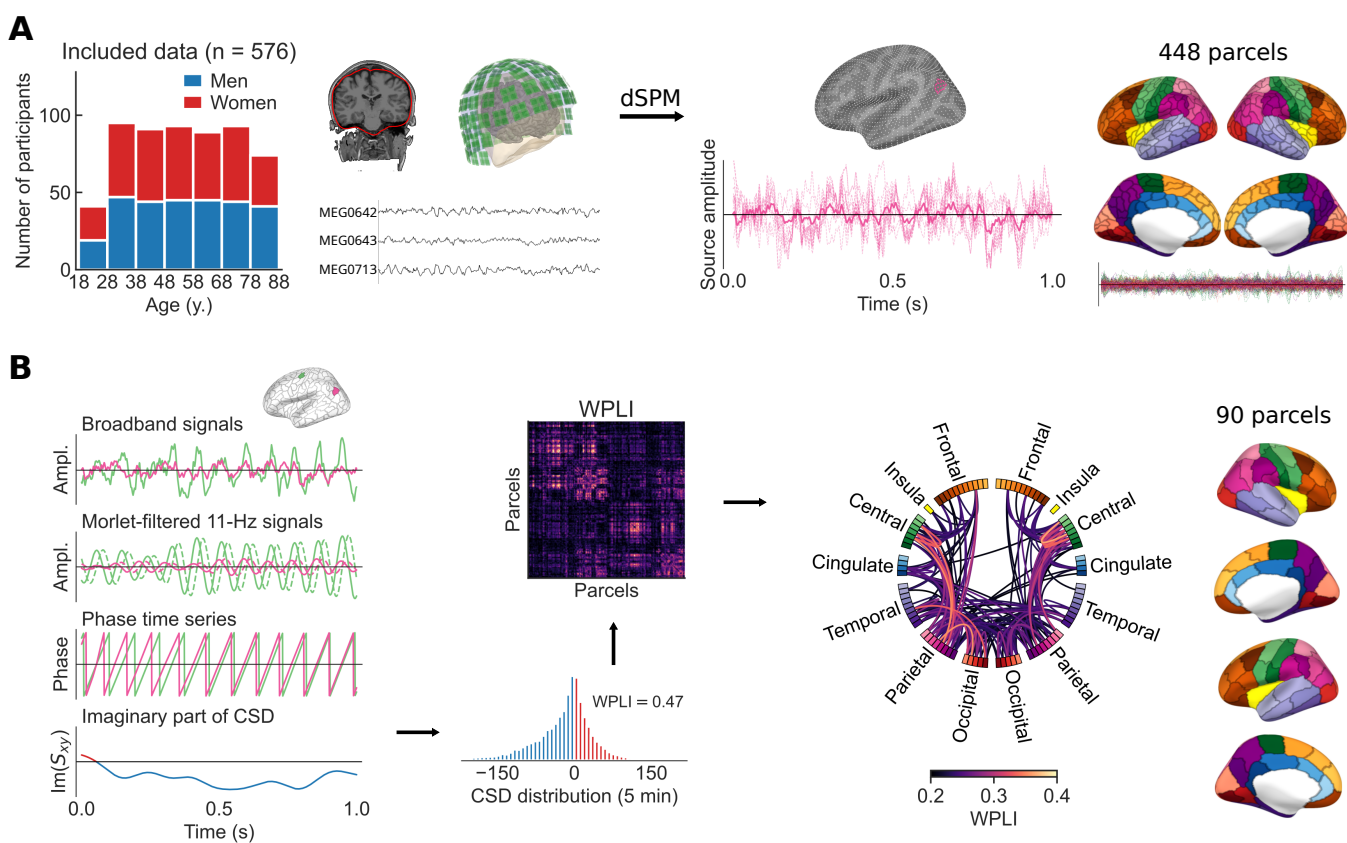


Figure 1. Data and analysis pipeline. (A) Resting-state MEG and structural MRI data from 576 healthy participants were used to extract neuronal source time courses at 5124 cortical source points. The source time courses were spatially averaged within 448 cortical regions of interest (ROIs) based on an anatomical parcellation. (B) Analytic signals in the 1–100-Hz frequency range were obtained using Morlet wavelet filtering, and the cross-spectral density (CSD) was calculated for each pair of ROIs. The imaginary part of CSD was used to calculate the Weighted Phase-Lag Index (WPLI) across time, resulting in a 448×448 all-to-all connectivity matrix. The WPLI values were spatially averaged within a sparser parcellation of 90 cortical regions, suitable for presentation in a circular graph.

connectivity analysis stems from source leakage, which may lead to false positive findings in the absence of true synchronization [18]. Several groups have utilized functional connectivity estimation methods highly susceptible to false positive findings due to source leakage, such as coherence and PLV. Second, some studies have been limited to sensor-level analyses, which accentuates the linear mixing between signals leading to spurious connectivity estimates and compromises the neurophysiological interpretability of the results [19]. Third, many previous studies have used coarse anatomical parcellations, which results in signal cancellation as source time courses are averaged within parcels. Finally, results on rs-FC could be confounded by concurrent changes in oscillatory source power, which affects functional connectivity estimates through altered signal-to-noise ratio [20].

The presence of putative age-related alterations in functional connectivity elicits interest in the potential connection between rs-FC and the maintenance of cognitive and sensorimotor function in older age. Age-related increases in functional connectivity during task performance and rest have generally been associated with the maintenance of cognitive performance, while decreased connectivity has been observed in patients with cognitive decline [9, 11, 21]. Most studies investigating age-related changes in rs-FC also report associations between cognitive performance and connectivity. In particular, reduced visual short-term memory (VSTM) performance has been related to decreased alpha-band global coherence and increased delta-band PLV variability in bilateral supramarginal regions [13, 14]. On the other hand, weaker performance in tasks testing fluid intelligence and visual memory has been reported with increased bilateral temporal lobe connectivity in the beta and gamma frequency ranges and reduced directed connectivity into posterior medial areas in the 1–100-Hz frequency range [12, 22]. Others have also reported associations between the similarity of structural and functional networks and higher performance in the mini-mental state evaluation [MMSE; 23] and VSTM tasks, suggesting that similar age-related reorganization of structural and functional connectivity has cognitive benefits [24].

65 Aging is typically associated with reduced sensory sensitivity [25]. The combination of perceived sensory stimuli and internal
66 forward models of movement is known as sensorimotor integration [26], where the contributions of sensory feedback and prediction
67 are weighted by their relative precision [27]. As a result, self-generated actions are perceived weaker than externally generated
68 actions [28]. This phenomenon is known as sensorimotor attenuation. Reduced sensory sensitivity with age leads to increased
69 reliance on prediction and, hence, to increased sensorimotor attenuation [29]. Anatomical and functional MRI data indicate that this
70 effect is associated with decreased gray matter volume in the supplementary motor area (pre-SMA) and decreased fMRI functional
71 connectivity between the pre-SMA and frontostriatal regions during both resting state and a movement task [29]. However, despite
72 the prominent role of beta oscillations in sensorimotor control [30, 31], the electrophysiological underpinnings of the age-related
73 increase in sensorimotor attenuation remain elusive.

74 The aims of the current study were twofold. First, we aimed to elucidate the trends of rs-FC across the healthy adult lifespan.
75 Specifically, we employed MEG to investigate the trajectories of source-space rs-FC across the healthy adult lifespan in the
76 Cam-CAN (Cambridge Centre for Ageing and Neuroscience) cohort [32, 33]. We analyzed resting-state MEG recordings from a
77 cross-sectional sample of 576 participants aged 18–87 years from the Cam-CAN database (**Fig 1A**). We addressed the common
78 methodological limitations including source leakage, suboptimal cortical parcellation, and confounding oscillatory power. To this
79 end, we estimated neuronal source time courses from preprocessed MEG data using the dynamic statistical parametric mapping
80 (dSPM) inverse method. We then estimated rs-FC between all pairs of 448 ROIs using weighted phase-lag index (WPLI) as
81 the connectivity metric in the theta (4–8 Hz), alpha (8–13 Hz), and beta (13–30 Hz) frequency bands (**Fig 1B**). We examined
82 the putative linear and nonlinear relationships between age and rs-FC using linear and quadratic association measures based on
83 hierarchical regression. Additionally, we analyzed age-related trends in neural source power to determine whether they mirrored
84 those of rs-FC, which would hinder the interpretation of changing rs-FC patterns as true changes of inter-areal connectivity.

85 Our second aim was to explore the potential role of rs-FC in the increased sensorimotor attenuation observed in older age
86 [29]. To this end, we analyzed the relationship between rs-FC and force overcompensation in a force matching task, which is
87 a well-established measure of sensorimotor attenuation. Given that beta-band connectivity during task performance has been
88 associated with accurate motor performance [34], we hypothesized that the baseline rs-FC levels could be indicative of performance
89 in the force matching task and reflect the efficient integration of sensory signals.

90 Results

91 Functional connectivity across the adult lifespan

92 We investigated age-related changes in rs-FC at the level of individual network connections. For visual inspection of rs-FC networks
93 across the adult lifespan, we averaged the estimated connectivity matrices across subjects within age cohorts in the theta (4–8 Hz),
94 alpha (8–13 Hz), and beta (13–30 Hz) frequency bands (**Fig 2B**). The averaged results showed distinct connectivity patterns in
95 each frequency band. In the theta band, the rs-FC networks were predominantly frontal–temporal. Alpha-band connectivity was
96 most prominent between the posterior and parietal regions. Notable beta-band rs-FC was observed between centroparietal areas.

97 To quantify age-related changes in rs-FC across the adult lifespan, we calculated linear and quadratic associations between
98 participant age and the strength of each connection in the rs-FC network in the theta, alpha, and beta frequency bands (**Fig 2C**). In
99 the theta band, we observed increased connectivity, particularly between frontal–temporal and frontal–occipital areas. Notably, a
100 large subset of the connections strengthening with age were interhemispheric. The largest effect size was observed between the left
101 medial orbitofrontal gyrus and the ROI consisting of the left cuneus and pericalcarine cortex ($\rho = 0.26$, $p_{FDR} = 0.003$). We also
102 found similar effects between frontal–temporal areas, including between the left frontal pole and the right middle temporal gyrus
103 ($\rho = 0.25$, $p_{FDR} = 0.003$). No significant quadratic associations were observed between the age of the participants and rs-FC in
104 the theta band.

105 In the alpha band, we identified linear age-related decreases in rs-FC, most prominently between temporal–occipital areas.
106 Some of the connections associated with the greatest effects were left fusiform gyrus b – left parahippocampal gyrus ($\rho = -0.27$,
107 $p_{FDR} = 0.004$), left lateral occipital b – left parahippocampal gyrus ($\rho = -0.26$, $p_{FDR} = 0.004$), and left lateral occipital a – left
108 fusiform a ($\rho = -0.26$, $p_{FDR} = 0.004$). The letters a and b here refer to the subdivision of Desikan–Killiany atlas parcels. We did
109 not observe significant quadratic associations between participant age and rs-FC in the alpha band.

110 In the beta-band, a general linear decrease in rs-FC was identified, with the strongest effects between posterior–parietal regions.
111 However, contrary to the alpha and theta bands, increased connectivity was observed in the frontal lobe. Some of the connections
112 exhibiting the strongest positive associations with age were left superior frontal gyrus b – left rostral middle frontal gyrus b
113 ($\rho = 0.22$, $p_{FDR} = 0.003$), and left lateral orbitofrontal gyrus – left rostral middle frontal gyrus b ($\rho = 0.22$, $p_{FDR} = 0.003$). The
114 largest decrease in connectivity with age was observed between areas in the occipital lobe: left lateral occipital cortex a – left
115 lingual gyrus b ($\rho = -0.37$, $p_{FDR} = 0.003$), and left cuneus and pericalcarine cortex – left lateral occipital cortex a ($\rho = -0.36$,
116 $p_{FDR} = 0.003$). The linear effect size was generally higher in the beta band compared to the alpha and theta frequency ranges.

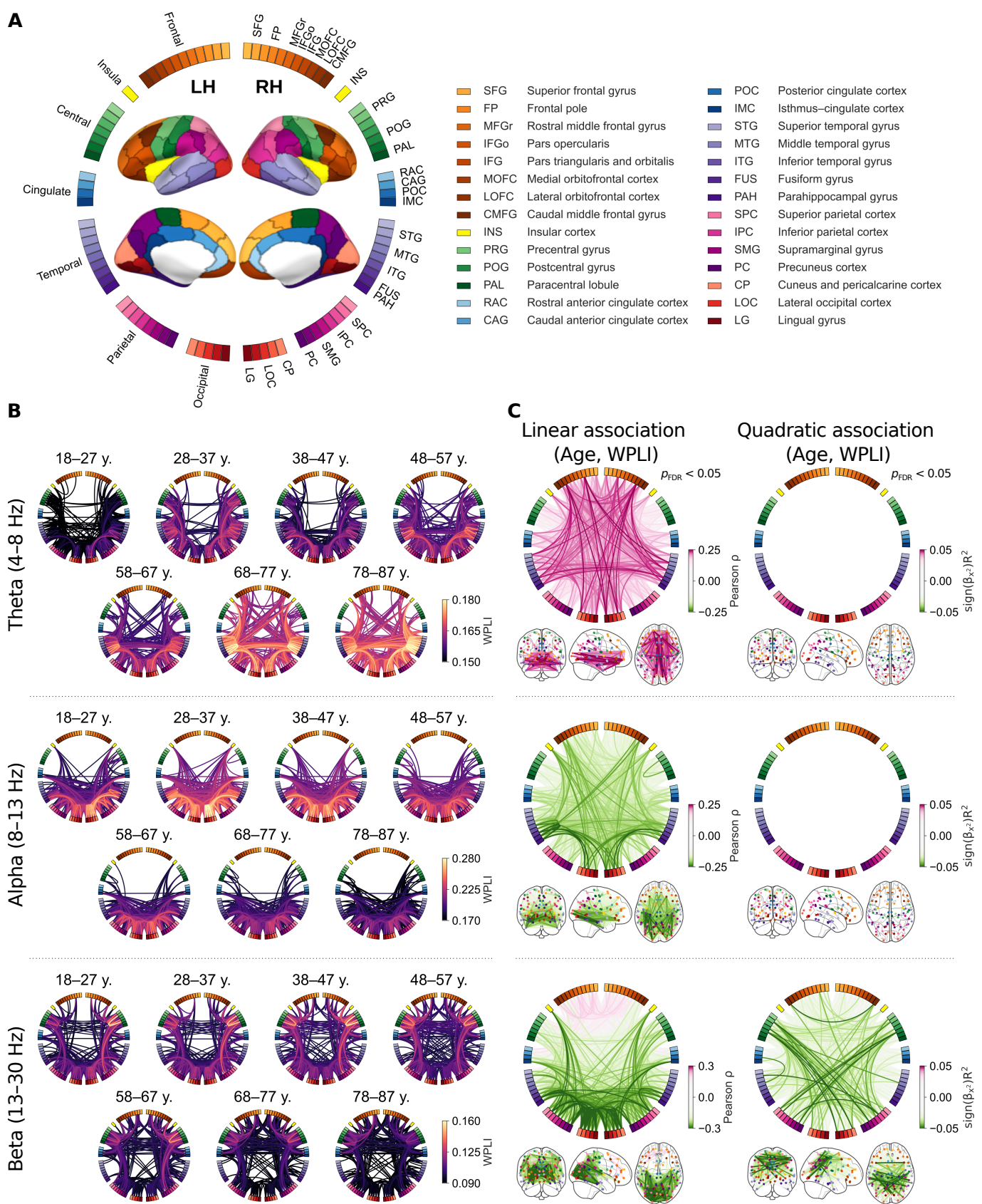


Figure 2. Functional connectivity changes across the adult lifespan. (A) Parcellation reference. All-to-all functional connectivity was estimated between 90 ROIs in an anatomical parcellation and visualized in circular connectivity plots. ROIs are placed around the circle and the lines between them represent connections in the network. (B) Group averages of functional connectivity within age cohorts in the theta (4–8 Hz), alpha (8–13 Hz), and beta (13–30 Hz) frequency bands show distinct frequency-dependent patterns. Each circular plot shows the 500 strongest links. (C) Linear (left column) and quadratic (right column) associations between participant age and connections strength reveal frequency-band-specific patterns of change across the adult lifespan. Each colored line in the figure represents the effect size of a significant association; the Pearson correlation coefficient for linear associations, and the coefficient of determination multiplied by the sign of the quadratic term coefficient for the quadratic associations. The circular plots and schematic brains provide complementary visual perspectives of the same data.

In addition to the decreasing linear trend, a negative quadratic relationship was identified between participant age and beta-band rs-FC, most notably between central-parietal and central-posterior areas. The negative quadratic trend corresponds to an inverted U-shape, indicating that these connections strengthen in young adults through middle age and decline in older adults toward later life. This pattern resembles those observed in structural connectivity and fMRI functional connectivity networks [4, 35]. Some of the strongest quadratic associations were observed between left and right caudal middle frontal gyri ($\text{sign}(\beta_{\text{age}^2}) \cdot R^2 = -0.054$, $p_{\text{FDR}} = 0.005$), left supramarginal gyrus a and right inferior parietal cortex ($\text{sign}(\beta_{\text{age}^2}) \cdot R^2 = -0.054$, $p_{\text{FDR}} = 0.005$), and left postcentral gyrus b and right lingual gyrus b ($\text{sign}(\beta_{\text{age}^2}) \cdot R^2 = -0.052$, $p_{\text{FDR}} = 0.005$).

Mean connectivity across the adult lifespan

To highlight age-related trends in rs-FC associated with individual brain regions, we calculated linear associations between the mean connectivity of each ROI and participant age in the theta, alpha, and beta frequency bands. We observed a general increase in mean connectivity with age in the theta band, particularly in frontal, temporal, and occipital areas (Fig 3). The strongest effect was observed bilaterally in the medial orbitofrontal cortices (left: $\rho = 0.23$, $p_{\text{FDR}} = 0.002$; right: $\rho = 0.22$, $p_{\text{FDR}} = 0.002$). In the alpha band, mean connectivity was negatively associated with age, and the effect was largest in the fusiform gyri (left: $\rho = -0.20$, $p_{\text{FDR}} = 0.003$; right: $\rho = -0.20$, $p_{\text{FDR}} = 0.003$). In the beta band, a more complex pattern showed age-related decreases in connectivity in the posterior and parietal regions combined with a modest positive trend in the frontal lobe. The largest effect size was associated with decreased connectivity of the bilateral superior parietal cortices (left: $\rho = -0.27$, $p_{\text{FDR}} = 0.002$; right: $\rho = -0.27$, $p_{\text{FDR}} = 0.002$).

Global connectivity and source power across the adult lifespan

To visualize and quantify age-related changes in whole-brain rs-FC across the 1–100-Hz frequency range, we calculated the linear and quadratic association spectra between participant age and global connectivity (Fig 4). We identified frequency-dependent patterns of both positive and negative linear and quadratic associations between age and global connectivity (Fig 4B). Generally, age and global connectivity were positively linearly associated at low frequencies below 7 Hz and high frequencies above 40 Hz. In contrast, a negative association was observed at intermediate frequencies (11–14 Hz and 20–23 Hz). The largest effect size was related to a negative association at 12 Hz ($\rho = -0.32$, $p_{\text{FDR}} = 0.002$), indicating reduced global connectivity with older age (Fig 4C). In addition to the linear trends across wide frequency ranges, we observed a negative quadratic association between age and global connectivity in a narrow 17–20-Hz range within the beta band, with the strongest effect at 17 Hz ($\text{sign}(\beta_{\text{age}^2})R^2 = -0.05$, $p_{\text{FDR}} = 0.016$).

To compare the adult lifespan trajectories of rs-FC to those of mere oscillatory power, we calculated the linear and quadratic association spectra between participant age and global source power (Fig 4E). We observed positive linear associations in low (1–2 Hz, 7 Hz) and high (14–100 Hz) frequencies. However, despite the associations between age and global connectivity, no significant linear relationships between age and global power were observed in the theta or alpha frequency ranges, except at 7 Hz. Positive quadratic associations between age and global source power were observed in low frequencies (1–6 Hz), again different from the frequency range where age and global connectivity were associated. This is illustrated in Fig 4C and Fig 4F, which highlight the absence of significant linear or quadratic associations between age and global source power at the frequencies of peak associations between age and global connectivity.

Beta-band connectivity and sensorimotor attenuation

To investigate the relationship between rs-FC and sensorimotor attenuation, we calculated linear associations between the mean force overcompensation in the force matching task and the mean connectivity of each ROI in the beta band. We identified significant negative associations in the centroparietal regions comprising sensorimotor cortices, indicating that increased overcompensation, and thus greater sensorimotor attenuation, is related to lower connectivity in those areas (Fig 5). In the left hemisphere, the strongest relationship was observed in the supramarginal gyrus ($\rho = -0.21$, $p_{\text{FDR}} = 0.022$). In the right hemisphere, the largest effect occurred in the postcentral gyrus ($\rho = -0.20$, $p_{\text{FDR}} = 0.022$).

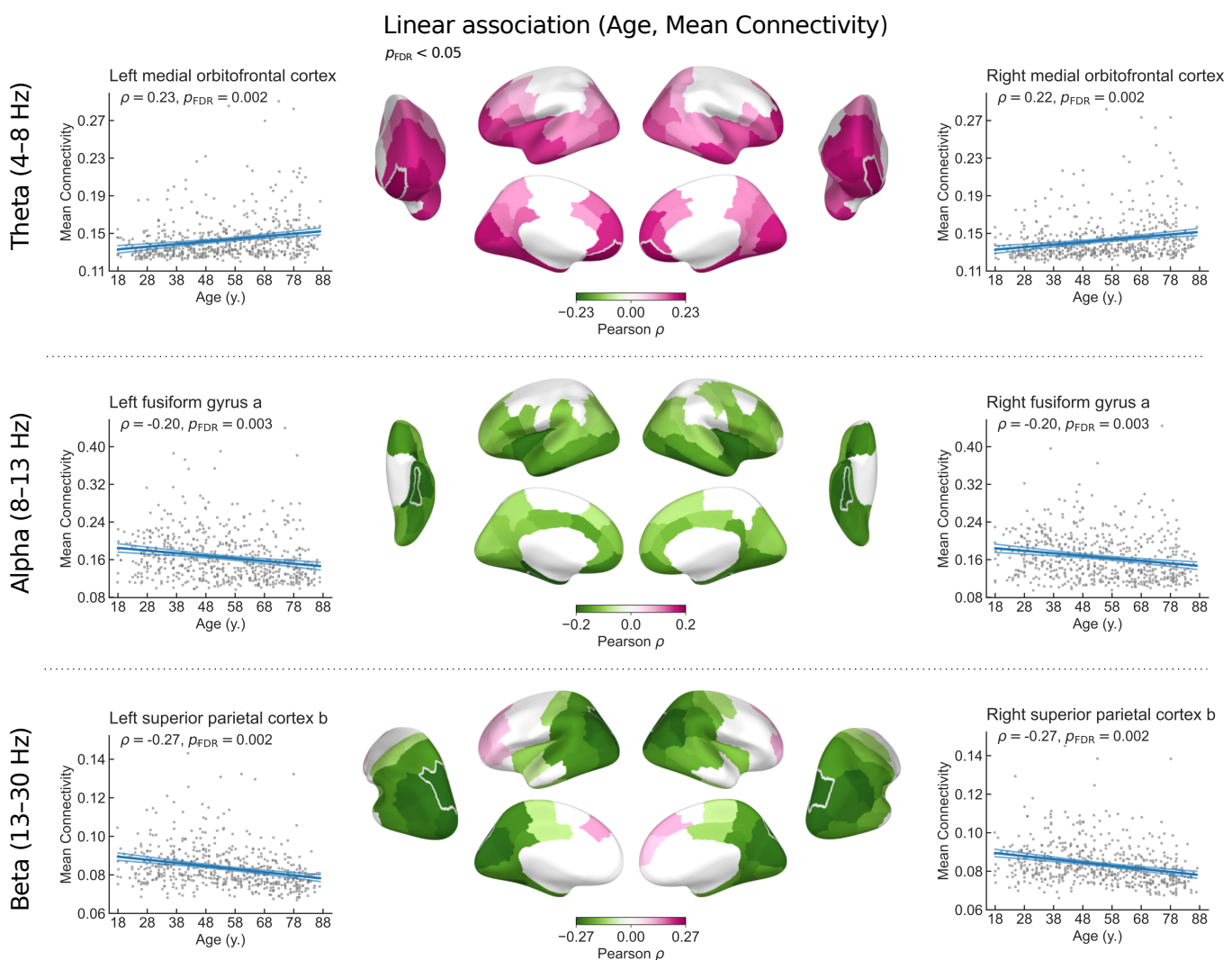


Figure 3. Mean connectivity changes across the adult lifespan. Brain regions showing significant associations between age and mean connectivity in the theta, alpha, and beta frequency bands are colored according to their Pearson correlation coefficient. The cortical areas associated with the largest effect sizes in each frequency band are highlighted with white borders. The scatter plots in the left and right columns illustrate the linear relationships between participant age and mean connectivity of the highlighted regions. Each data point represents an individual subject. The lower intensity lines show the 95% confidence intervals.

160 Discussion

161 In this study, we aimed to elucidate the trends of resting-state functional connectivity (rs-FC) across the healthy adult lifespan and
 162 the potential role of rs-FC in sensorimotor integration. Our results revealed frequency-dependent rs-FC trajectories as a function of
 163 age. We also showed a linear relationship between the beta-band rs-FC and sensorimotor attenuation, indicating that the ongoing
 164 inter-areal synchronization in the beta band is involved in sensorimotor integration. Furthermore, we showed that rs-FC and source
 165 power have distinct frequency-dependent trajectories, suggesting that rs-FC provides additional information to that conveyed by
 166 source power alone.

167 In the beta band, our analysis of rs-FC network connections across the lifespan showed a linear age-related decrease in rs-FC
 168 between posterior and parietal regions. The observed effect size was larger in the beta band compared to the alpha and theta
 169 frequency ranges. In addition to the linear trend, we observed an age-related negative quadratic "inverted U-shape" trend between
 170 centroparietal regions, similar to what has been reported within resting-state networks in fMRI [4], white matter volume [1], and
 171 structural connectivity [35]. Notably, the linear and quadratic associations showed distinct spatial patterns, hinting that separate
 172 underlying mechanisms could drive these changes within the same frequency band. In general, the age-related patterns observed

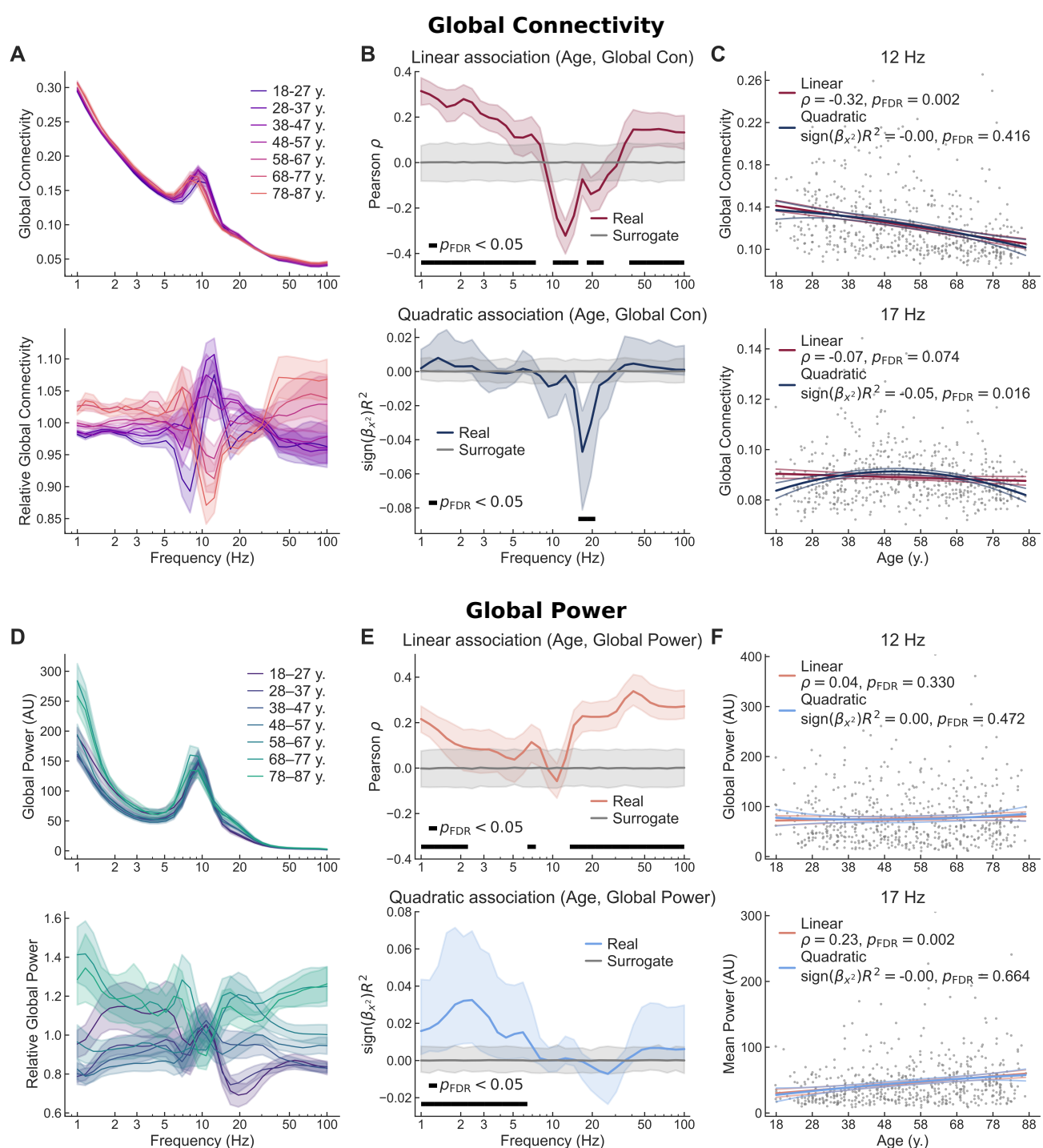


Figure 4. Global connectivity and source power change across the adult lifespan. (A) Group averages of absolute (top) and relative (bottom) global connectivity spectrum within age cohorts. Shaded areas indicate the standard error of the mean. (B) Linear (top) and quadratic (bottom) association spectra between participant age and global connectivity. Shaded areas indicate 95% bootstrap confidence intervals. (C) Scatter plots of global connectivity as a function of participant age at 12 Hz (top) and 17 Hz (bottom) show the peak linear and quadratic relationships, respectively. The lower intensity lines show the 95% confidence intervals. (D) Group averages of absolute (top) and relative (bottom) mean source power within age cohorts. (E) Linear (top) and quadratic (bottom) association spectra between participant age and mean source power. (F) Scatter plots of mean source power as a function of participant age at 12 Hz (top) and 17 Hz (bottom) show non-significant or opposing trends compared to global connectivity.

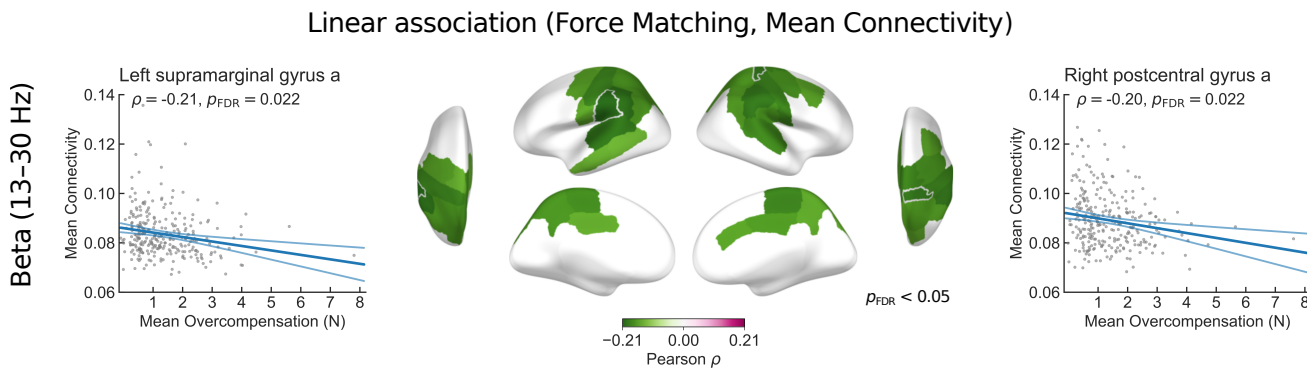


Figure 5. Association between mean connectivity and performance in a force matching task. Brain regions showing significant negative linear associations between beta-band mean connectivity and mean force overcompensation in the force matching task are depicted in green. The scatter plots present data from the regions with the strongest observed correlations—the left supramarginal gyrus and the right postcentral gyrus. The lower intensity lines show the 95% confidence intervals.

at the ROI level align with the results of a recent study by Stier and colleagues [15] despite some methodological differences, increasing our confidence in the replicability of the results.

Beta-band oscillatory activity is central to sensorimotor control and has been associated with maintaining the current sensorimotor state [30, 31]. Aging has previously been associated with increased sensorimotor attenuation, which could be attributed to increased reliance on sensorimotor prediction as opposed to sensory feedback [29]. Moreover, increased sensorimotor attenuation has been associated with increased fMRI functional connectivity between the supplementary motor area (pre-SMA) and the primary somatosensory cortex, along with decreased functional connectivity between the pre-SMA and frontostriatal areas [29]. To investigate the underlying neuronal dynamics, we analyzed the relationship between rs-FC and mean overcompensation in the force matching task. In contrast to the fMRI findings, we observed an association between decreased connectivity of the broader sensorimotor areas in the beta band and increased force overcompensation. This association suggests that a higher level of beta-band functional connectivity at rest could be indicative of efficient sensory information processing, leading to less pronounced sensorimotor attenuation, whereas decreased beta-band connectivity could be related to increased sensory noise and greater emphasis on internal predictive models, observed as increased sensorimotor attenuation. Considering that aging was related to decreased connectivity in the beta band, this interpretation would align with previous observations of increased sensory noise and improved sensorimotor prediction in healthy aging [25, 36].

In the alpha band, our results showed an overall decrease in rs-FC with age, prominently between frontal, temporal, and occipital areas. At the ROI level, the strongest associations between age and mean connectivity were observed in the fusiform and parahippocampal gyri in the medial temporal lobe along with weaker effects in the wider frontal, temporal, and occipital areas. These results agree with a previous study that observed an age-related decrease in temporal lobe connectivity in the same cohort [15]. Although reduced alpha-band rs-FC has previously been associated with reduced VSTM precision in healthy aging [13] and is widely considered a marker of mild cognitive impairment and Alzheimer's disease [8, 9, 11, 37], it remains challenging to interpret the neurophysiological mechanisms underlying these changes. Nevertheless, given that alpha-band connectivity between task relevant regions has been suggested to have a facilitating role in visual memory [38], these changes could explain the age-related decline in VSTM precision.

It is well known that the frequency of the individual alpha peak decreases throughout the adult lifespan from approximately 10 Hz in young adulthood to less than 9 Hz in the elderly [39, 40], although considerable inter-individual variability is involved [41]. The decrease of the peak alpha frequency is a possible confounding factor in functional connectivity analysis, as the strongest connectivity is typically observed at the peak frequency [40]. Age-related changes in source power could also lead to biased estimates of age-related changes in connectivity since higher source power translates to a higher signal-to-noise ratio (SNR), and it is known that variations in SNR are a major source of bias in functional connectivity analysis [20, 42]. Although prior work suggests age-related increases in MEG source power in the alpha band [5, 15], we did not observe age-related trends in global power in that frequency range despite an observed decrease in global connectivity. These results together suggest that our rs-FC findings in the alpha band are not merely echoes of altered source power. Similarly, we observed no significant linear changes in theta power with age, and only a linear increase in beta power despite both negative linear and negative quadratic trends in rs-FC.

In our analysis of age-related changes in all-to-all connectivity, we observed a positive linear association between participant age and theta-band rs-FC between frontal–temporal and frontal–occipital areas, with a notable degree of interhemispheric coupling.

209 This was mirrored by the ROI-level mean connectivity results, which showed increased connectivity in frontal, temporal, and
210 occipital areas with the largest effects in the bilateral medial orbitofrontal cortices. These results are in line with a previous study
211 from Stier and colleagues [15], although our results suggest a more pronounced role for the frontal cortex. Theta-band connectivity,
212 particularly that of the medial prefrontal cortex, has been credited with a central mediating role in cognitive control and working
213 memory through the entrainment of distal regions [43–45]. These effects have been observed mainly during task performance,
214 and it has also been suggested that the level of theta rs-FC could reflect the functioning of attentional mechanisms [46]. Despite
215 these findings, there is a lack of consensus regarding the role of theta-band connectivity in cognitive aging. While some studies
216 have associated increased theta connectivity with a compensatory role in cognitive aging, others have associated it with decreased
217 cognitive performance [21].

218 Although we addressed most of the methodological concerns inherent to resting-state functional connectivity, one should
219 be aware of a few remaining limitations upon interpreting the results. First, although the applied connectivity metric, Weighted
220 Phase-Lag Index (WPLI), is insensitive to instantaneous synchronization and resilient against noise [47], spurious interactions
221 between sources near the truly interacting sources could remain in the results [18]. This limitation should be considered when
222 interpreting the observed spatial patterns. Another potential confounding factor arises from the uncontrolled nature of resting-state
223 measurements; it is not well understood how the internal cognitive state and vigilance of the participant affect rs-FC. Finally,
224 the large interindividual variability observed in our study could limit the interpretability of rs-FC analysis at the individual level.
225 Nevertheless, the use of large MEG datasets enables modeling of the normal healthy variability in functional connectivity, which
226 could lead to improved diagnostics and prognosis of brain disorders [48]. Our demonstration of age-related variability in rs-FC
227 emphasizes the importance of age-stratified normative modeling.

228 Our study contributes to the literature on healthy aging with three main findings. First, we showed that resting-state functional
229 connectivity (rs-FC), quantified as phase coupling between spontaneous cortical oscillations, is altered in healthy aging. The
230 observed changes showed different spatial patterns in the theta, alpha, and beta frequency bands. In the beta band, rs-FC followed
231 an inverted U-shape trajectory with age, mirroring patterns previously observed in MRI studies of structural and functional
232 connectivity. Second, we showed that the global trends in rs-FC differ from those of oscillatory source power, alleviating concerns
233 that the age-related changes in rs-FC would be confounded by changes in source power. Finally, our results indicate an association
234 between reduced beta-band rs-FC in sensorimotor areas and increased sensorimotor attenuation, which suggests that rs-FC plays a
235 role in the integration of sensory signals and internal predictive models. In summary, our results contribute to the understanding of
236 the role of brain oscillations in healthy aging and open new avenues for future studies linking the observed changes in rs-FC with
237 behavior and cognition, as well as further elucidating the putative role of beta-band rs-FC in sensorimotor integration.

238 Methods

239 Participants and recordings

240 The data were collected at the Medical Research Council (UK) Cognition and Brain Sciences Unit (MRC-CBSU) in Cambridge,
241 UK, as part of the Cambridge Center for Ageing and Neuroscience (Cam-CAN) study [32, 33]. The cross-sectional, multimodal
242 open-access database includes structural and functional MRI, MEG, and behavioral recordings of a population-based cohort of
243 nearly 700 healthy participants aged between 18 and 88 years with an approximately uniform age distribution. The participants
244 were selected for neuroimaging and detailed behavioral experiments following an initial screening stage that assessed general and
245 cognitive health. The inclusion criteria comprised normal cognitive health, no serious psychiatric conditions, meeting hearing and
246 English language requirements, and no contraindications for MRI recordings (for details, see [32]). In our primary analysis, we
247 included $n = 576$ participants after excluding participants due to missing anatomical MRI or resting-state MEG data, poor data
248 quality, missing head position indicator (HPI) signals or electrooculogram (EOG) channels, and failed FreeSurfer reconstructions
249 (**Fig 1A**). To investigate the relationship between functional connectivity and sensorimotor attenuation, we included a subset
250 of $n = 284$ participants with available recordings from the force matching task collected in the Cam-CAN study. The primary
251 study was conducted in accordance with the Declaration of Helsinki and was approved by the Cambridgeshire 2 Research Ethics
252 Committee (reference: 10/H0308/50). The participants gave written informed consent.

253 MRI data were collected at MRC-CBSU using a 3-T Siemens TIM Trio scanner (Siemens Healthineers AG, Munich, Germany)
254 and a 32-channel head coil. T1-weighted scans were collected using a magnetization-prepared gradient echo sequence with the
255 following parameters: repetition time 2250 ms, echo time 2.99 ms, flip angle 9°, and inversion time 900 ms. MEG data were
256 recorded in the seated position during rest (eyes closed) using a 306-channel VectorView MEG system (MEGIN Oy, Espoo, Finland)
257 at MRC-CBSU. Horizontal and vertical EOG and single-lead electrocardiogram (ECG) were recorded simultaneously with MEG.
258 The head position of the participant was continuously monitored using four HPI coils. The duration of the resting-state recording
259 was 8 minutes and 40 seconds. Data were bandpass-filtered to 0.03–330 Hz and sampled at 1 kHz. Further details on the MRI and
260 MEG data acquisition are available in the publication by Taylor and colleagues [33].

261 The force matching task, which quantifies sensorimotor attenuation, was performed in a separate session from the neuroimaging
262 measurements by half of the neuroimaging participants [32]. In the experimental setting, a torque motor attached to a lever was

263 used to apply a target force to the participant's left index finger, which rested below the lever. Following concurrent auditory and
264 visual cues, the participant attempted to match the target force with their right index finger either by directly pressing on the lever
265 (direct condition) or by operating a linear potentiometer connected to the torque motor (indirect condition). A force sensor attached
266 to the lever recorded both the target and matched forces. The experiment included 32 trials for each condition. The mean difference
267 between the target and matched forces in each condition is called mean overcompensation. Positive values in the direct condition
268 indicate sensorimotor attenuation, while the indirect condition serves as a control for the sensitivity of haptic pressure perception
269 [29]. In our analysis, we only considered the direct condition as a proxy of the extent of sensorimotor attenuation.

270 **MEG preprocessing**

271 We followed standard MEG analysis practices, consisting of data preprocessing, coregistration with structural MRI, and estimation
272 of neural current sources in a source space based on individual brain anatomy. The analysis was performed primarily using
273 MNE-Python software version 1.6 [49, 50].

274 Spatiotemporal signal-space separation [tSSS; 51] was employed to remove external interference and compensate for head
275 movement during the measurement (MaxFilter v2.3 (Megin Oy, Espoo, Finland); correlation limit 0.98; correlation window length
276 10 s). Data were bandpass-filtered to 1–100 Hz and notch-filtered at the 50-Hz line frequency and harmonics. The same procedure
277 was applied to the resting-state and empty-room data, except for head movement correction. Independent Component Analysis
278 (ICA) was used to dampen artifacts arising from eye movement and cardiac activity [FastICA; 52]. Independent components
279 were automatically selected for removal based on their Pearson correlation with the EOG channels and cross-trial phase statistics
280 with the ECG channel [53]. Following artifact removal, the MEG data were divided into 30-s epochs, and any epochs containing
281 residual artifacts were rejected based on peak-to-peak amplitude thresholds (magnetometers: 10 pT; gradiometers: 10 pT/cm). The
282 first 10 good 30-s epochs for each subject were included in the subsequent analysis for a total recording duration of 5 min. Subjects
283 with less than 10 good epochs were excluded from further analysis, resulting in a sample size of $n = 576$.

284 **MRI processing and forward model**

285 T1-weighted structural MRI data were used to create 3-D cortical reconstructions of each participant using FreeSurfer software
286 [54, 55]. For the MEG forward model, we used a single-compartment linear collocation boundary element method (BEM) volume
287 conductor model. The intracranial volume boundary tessellation was obtained through the FreeSurfer watershed algorithm [56].
288 A cortically-constrained source space with recursively subdivided icosahedron spacing (ico4) was defined for each participant,
289 resulting in 5124 cortical source points. The anatomical data were manually coregistered with the MEG measurements using the
290 MNE-Python coregistration GUI. The MEG–MRI coregistrations were provided by Bardouille and colleagues [57].

291 **Source estimation**

292 We estimated the time courses of neuronal activation using the dynamic statistical parametric mapping [dSPM; 58] inverse
293 method (regularization parameter 0.111; depth-weighting exponent 0.8; loose orientation constraint 0.2 [59]). We used the sample
294 covariance method to estimate noise covariance matrices from empty-room recordings measured in the same session with the
295 recording of each participant. Source time courses were estimated at the 5124 cortical source points and morphed into the
296 FreeSurfer *fsaverage* reference brain template to facilitate analysis across subjects. Both magnetometers and gradiometers were
297 used in source estimation.

298 **Cortical parcellation**

299 To decrease computational complexity and increase interpretability, we employed a cortical parcellation to reduce the dimensionality
300 of the source-space data. To that end, the data were organized into 448 ROIs as defined in the *aparc_sub* parcellation scheme
301 developed by Khan and colleagues [60] based on the Desikan–Killiany atlas [61] (**Fig 1A**). The time courses within each ROI were
302 then averaged to form a representative time series. To prevent signal cancellation at the opposite sides of sulci, a sign-flip operation
303 was applied to the signals of the sources whose orientation differed from the dominant direction within the ROI by more than 90°.
304 The use of a relatively dense parcellation further reduces signal cancellation and flattening during the averaging procedure.

305 **Morlet wavelet filtering**

306 Pairwise phase-based functional connectivity metrics can be computed from the cross-spectral density between two analytic signals,
307 each representing the activation of an ROI across time and frequency. To obtain the analytic signals, we applied Morlet wavelet
308 filtering to the ROI representative time series (**Fig 1B**). The ROI time series were convolved with complex Morlet wavelets with the
309 Morlet parameter $\omega = 5$, and 32 logarithmically spaced central frequencies between 1 and 100 Hz. The resulting analytic signals
310 were used to calculate both the source power at each ROI and the cross-spectral density between all pairs of ROIs.

311 **Functional connectivity analysis**

312 Inter-areal synchronization between neuronal oscillations provides a mechanism for functional connectivity between neuronal
313 populations [62, 63]. The degree of functional connectivity can be quantified by evaluating the consistency of the phase
314 difference between two oscillatory signals representing spatially separated brain areas. We estimated all-to-all pairwise functional
315 connectivity between the 448 ROIs using the Weighted Phase-Lag Index (WPLI) as the connectivity metric [47]. WPLI quantifies
316 the asymmetry of the phase-difference distribution between a pair of signals over time, weighted by the magnitude of the
317 imaginary part of the cross-spectral density. The WPLI formulation minimizes both the influence of artificial interactions due
318 to source leakage and the sensitivity to noise [47]. We applied the implementation in MNE-Connectivity software version 0.5
319 (<https://mne.tools/mne-connectivity/>).

320 We computed WPLI separately in each frequency bin and averaged the results across frequencies within the canonical theta
321 (4–8 Hz), alpha (8–13 Hz), and beta (13–30 Hz) frequency bands. To reduce the dimensionality of the 448×448 connectivity
322 matrices, we employed a sparser custom parcellation of 90 ROIs in the ROI- and connection-level analyses (**Fig 1B**). The custom
323 parcellation was created by grouping parcels from the 448-ROI *aparc_sub* parcellation [60] in a way that avoids elongated
324 regions, thereby minimizing signal cancellation while maintaining a homogeneous parcel size across the brain and facilitating
325 interpretable visualizations. This process resulted in an intermediate granularity between the *aparc_sub* parcellation and the original
326 Desikan–Killiany atlas [61], improving the anatomical interpretability of the involved cortical areas while limiting the overall
327 number of connections in the subsequent statistical analysis. The 448×448 connectivity matrices were transformed into the sparser
328 parcellation by spatially averaging the connectivity scores within each of the 90 ROIs, yielding 90×90 matrices. These matrices
329 constitute the adjacency matrices of the weighted connectivity networks (**Fig 1B**). In addition to analyzing individual connections,
330 we considered the mean connectivity of each ROI, which we defined as the mean strength of the connections associated with the
331 ROI. Furthermore, we analyzed age-related changes in global connectivity defined as the mean of all connections in the connectivity
332 network.

333 **Permutation statistics of linear and quadratic associations**

334 We investigated the trajectories of functional connectivity across the adult lifespan at three levels: individual connections in the
335 connectivity network, mean connectivity of each ROI, and global connectivity across the whole network. To visually inspect
336 age-related trends, we averaged the connectivity matrices and global connectivity across subjects within each age decade. Given
337 that age-related phenomena are often nonlinear, we assessed both linear and quadratic associations between participant age,
338 functional connectivity, source power, and overcompensation in the force matching task.

339 We modeled linear and quadratic associations using hierarchical linear regression. First, we fit a simple linear regression model
340 with age as the independent variable to quantify linear associations. At the second level, we considered quadratic associations
341 after removing the linear trend, adding age squared as an independent variable. We evaluated the statistical significance of the
342 associations using a nonparametric two-tailed permutation test. We indexed the effect size of the linear associations using the
343 Pearson correlation coefficient and that of the quadratic associations using the model coefficient of determination multiplied by the
344 sign of the quadratic term coefficient, which were used as test statistics in the permutation test. The permutation distribution was
345 obtained by shuffling the dependent variable vectors ($n_{\text{permutations}} = 1000$). This is equivalent to the null hypothesis that the model
346 does not explain any variance in the data (i.e., the coefficient of determination is zero).

347 We leveraged a mass univariate approach to analyze the associations between participant age and functional connectivity at the
348 level of individual connections in the connectivity network, fitting separate hierarchical regression models for each connections.
349 The number of subjects was $n = 576$. This resulted in 3960 fitted hierarchical regression models per frequency band. For mean
350 connectivity, a similar approach resulted in 90 fitted models per frequency band. In addition to evaluating the association between
351 participant age and local connectivity, we also assessed the relationship between overcompensation in the force matching task and
352 mean connectivity ($n = 284$). At the whole network level, we fit separate models for each log-spaced frequency bin to provide
353 an association spectrum across the entire 1–100-Hz frequency range, resulting in 32 fitted models. In addition to examining the
354 dependency between age and global connectivity, we also analyzed the relationship between age and mean source power. We
355 corrected all results for multiple comparisons by applying false discovery rate correction [FDR; 64] separately at each analysis
356 level. At the connection and ROI levels, p-values were pooled across connections and regions within frequency bands, whereas at
357 the whole network level, they were pooled across frequency bins.

358 **Data availability**

359 The original MEG, MRI, and behavioral data are available upon request from the Cam-CAN data repository (<https://camcan-archive.mrc-cbu.cam.ac.uk//dataaccess/>).

361 **Code availability**

362 The code developed and used in this study is available from the corresponding author upon request.

363 References

- [1] Bethlehem, R. A. I. *et al.* Brain charts for the human lifespan. *Nature* **604**, 525–533 (2022).
- [2] Damoiseaux, J. S. *et al.* Reduced resting-state brain activity in the "default network" in normal aging. *Cereb. Cortex* **18**, 1856–1864 (2008).
- [3] Ferreira, L. K. & Busatto, G. F. Resting-state functional connectivity in normal brain aging. *Neurosci. Biobehav. Rev.* **37**, 384–400 (2013).
- [4] Betzel, R. F. *et al.* Changes in structural and functional connectivity among resting-state networks across the human lifespan. *NeuroImage* **102**, 345–357 (2014).
- [5] Rempe, M. P. *et al.* Spontaneous cortical dynamics from the first years to the golden years. *Proc. Natl. Acad. Sci.* **120**, e2212776120 (2023).
- [6] Stam, C. J. Use of magnetoencephalography (MEG) to study functional brain networks in neurodegenerative disorders. *J. Neurol. Sci.* **289**, 128–134 (2010).
- [7] Stoffers, D. *et al.* Increased cortico-cortical functional connectivity in early-stage Parkinson's disease: An MEG study. *NeuroImage* **41**, 212–222 (2008).
- [8] Stam, C. *et al.* Magnetoencephalographic evaluation of resting-state functional connectivity in Alzheimer's disease. *NeuroImage* **32**, 1335–1344 (2006).
- [9] Mandal, P. K., Banerjee, A., Tripathi, M. & Sharma, A. A comprehensive review of magnetoencephalography (MEG) studies for brain functionality in healthy aging and Alzheimer's disease (AD). *Front. Comput. Neurosci.* **12** (2018).
- [10] Vlahou, E. L., Thurm, F., Kolassa, I.-T. & Schlee, W. Resting-state slow wave power, healthy aging and cognitive performance. *Sci. Rep.* **4**, 5101 (2014).
- [11] Buzi, G., Fornari, C., Perinelli, A. & Mazza, V. Functional connectivity changes in mild cognitive impairment: A meta-analysis of M/EEG studies. *Clin. Neurophysiol.* **156**, 183–195 (2023).
- [12] Schlee, W., Leirer, V., Kolassa, I.-T., Weisz, N. & Elbert, T. Age-related changes in neural functional connectivity and its behavioral relevance. *BMC Neurosci.* **13**, 16 (2012).
- [13] Sahoo, B., Pathak, A., Deco, G., Banerjee, A. & Roy, D. Lifespan associated global patterns of coherent neural communication. *NeuroImage* **216**, 116824 (2020).
- [14] Jauny, G., Eustache, F. & Hinault, T. Connectivity dynamics and cognitive variability during aging. *Neurobiol. Aging* **118**, 99–105 (2022).
- [15] Stier, C., Braun, C. & Focke, N. K. Adult lifespan trajectories of neuromagnetic signals and interrelations with cortical thickness. *NeuroImage* **278**, 120275 (2023).
- [16] Doval, S., Nebreda, A. & Bruña, R. Functional connectivity across the lifespan: a cross-sectional analysis of changes. *Cereb. Cortex* **34**, bhae396 (2024).
- [17] Coquelet, N. *et al.* The electrophysiological connectome is maintained in healthy elders: a power envelope correlation MEG study. *Sci. Rep.* **7**, 13984 (2017).
- [18] Palva, J. M. *et al.* Ghost interactions in MEG/EEG source space: A note of caution on inter-areal coupling measures. *NeuroImage* **173**, 632–643 (2018).
- [19] Schoffelen, J.-M. & Gross, J. Source connectivity analysis with MEG and EEG. *Hum. Brain Mapp.* **30**, 1857–1865 (2009).
- [20] Donoghue, T., Schawronkow, N. & Voytek, B. Methodological considerations for studying neural oscillations. *Eur. J. Neurosci.* **55**, 3502–3527 (2022).
- [21] Jauny, G., Eustache, F. & Hinault, T. T. M/EEG dynamics underlying reserve, resilience, and maintenance in aging: A review. *Front. psychol.* **13** (2022).
- [22] Schlee, W. *et al.* Development of large-scale functional networks over the lifespan. *Neurobiol. Aging* **33**, 2411–2421 (2012).
- [23] Folstein, M. F., Folstein, S. E. & McHugh, P. R. "Mini-mental state". A practical method for grading the cognitive state of patients for the clinician. *J. Psychiatr. Res.* **12**, 189–198 (1975).
- [24] Jauny, G. *et al.* Linking structural and functional changes during aging using multilayer brain network analysis. *Commun. Biol.* **7**, 239 (2024).
- [25] Konczak, J. *et al.* Parkinson's disease accelerates age-related decline in haptic perception by altering somatosensory integration. *Brain* **135**, 3371–3379 (2012).
- [26] Wolpert, D. M., Ghahramani, Z. & Jordan, M. I. An internal model for sensorimotor integration. *Science* **269**, 1880–1882 (1995).
- [27] Kording, K. P. & Wolpert, D. M. Bayesian integration in sensorimotor learning. *Nature* **427**, 244–247 (2004).
- [28] Chapman, C., Bushnell, M., Miron, D., Duncan, G. & Lund, J. Sensory perception during movement in man. *Exp. Brain Res.* **68** (1987).
- [29] Wolpe, N. *et al.* Ageing increases reliance on sensorimotor prediction through structural and functional differences in frontostriatal circuits. *Nat. Commun.* **7**, 13034 (2016).

- [30] Engel, A. K. & Fries, P. Beta-band oscillations — signalling the status quo? *Curr. Opin. Neurobiol.* **20**, 156–165 (2010).
- [31] Barone, J. & Rossiter, H. E. Understanding the role of sensorimotor beta oscillations. *Front. syst. neurosci.* **15**, 655886 (2021).
- [32] Shafto, M. *et al.* The Cambridge Centre for Ageing and Neuroscience (Cam-CAN) study protocol: A cross-sectional, lifespan, multidisciplinary examination of healthy cognitive ageing. *BMC Neurology* **14** (2014).
- [33] Taylor, J. R. *et al.* The Cambridge Centre for Ageing and Neuroscience (Cam-CAN) data repository: Structural and functional MRI, MEG, and cognitive data from a cross-sectional adult lifespan sample. *NeuroImage* **144**, 262–269 (2017).
- [34] Chung, J. W., Ofori, E., Misra, G., Hess, C. W. & Vaillancourt, D. E. Beta-band activity and connectivity in sensorimotor and parietal cortex are important for accurate motor performance. *NeuroImage* **144**, 164–173 (2017).
- [35] Zhao, T. *et al.* Age-related changes in the topological organization of the white matter structural connectome across the human lifespan. *Hum. Brain Mapp.* **36**, 3777 (2015).
- [36] Moran, R. J., Symmonds, M., Dolan, R. J. & Friston, K. J. The brain ages optimally to model its environment: Evidence from sensory learning over the adult lifespan. *PLoS Comput. Biol.* **10**, e1003422 (2014).
- [37] López, M. E. *et al.* Synchronization during an internally directed cognitive state in healthy aging and mild cognitive impairment: a MEG study. *AGE* **36**, 1389–1406 (2014).
- [38] Palva, J. M., Monto, S., Kulasekhar, S. & Palva, S. Neuronal synchrony reveals working memory networks and predicts individual memory capacity. *Proc. Natl. Acad. Sci.* **107**, 7580–7585 (2010).
- [39] Klimesch, W. EEG alpha and theta oscillations reflect cognitive and memory performance: a review and analysis. *Brain Res. Rev.* **29**, 169–195 (1999).
- [40] Scally, B., Burke, M. R., Bunce, D. & Delvenne, J.-F. Resting-state EEG power and connectivity are associated with alpha peak frequency slowing in healthy aging. *Neurobiol. Aging* **71**, 149–155 (2018).
- [41] Haegens, S., Cousijn, H., Wallis, G., Harrison, P. J. & Nobre, A. C. Inter- and intra-individual variability in alpha peak frequency. *NeuroImage* **92**, 46–55 (2014).
- [42] Bastos, A. M. & Schoffelen, J.-M. A tutorial review of functional connectivity analysis methods and their interpretational pitfalls. *Front. syst. neurosci.* **9** (2016).
- [43] Cavanagh, J. F. & Frank, M. J. Frontal theta as a mechanism for cognitive control. *Trends Cogn. Sci.* **18**, 414–421 (2014).
- [44] Liebe, S., Hoerzer, G. M., Logothetis, N. K. & Rainer, G. Theta coupling between V4 and prefrontal cortex predicts visual short-term memory performance. *Nat. Neurosci.* **15**, 456–462 (2012).
- [45] Daume, J., Graetz, S., Gruber, T., Engel, A. K. & Friese, U. Cognitive control during audiovisual working memory engages frontotemporal theta-band interactions. *Sci. Rep.* **7**, 12585 (2017).
- [46] Fellrath, J., Mottaz, A., Schnider, A., Guggisberg, A. G. & Ptak, R. Theta-band functional connectivity in the dorsal fronto-parietal network predicts goal-directed attention. *Neuropsychologia* **92**, 20–30 (2016).
- [47] Vinck, M., Oostenveld, R., van Wingerden, M., Battaglia, F. & Pennartz, C. M. An improved index of phase-synchronization for electrophysiological data in the presence of volume-conduction, noise and sample-size bias. *NeuroImage* **55**, 1548–1565 (2011).
- [48] Itäläinen, V., Kaltainen, H., Forss, N., Liljeström, M. & Parkkonen, L. Using normative modeling and machine learning for detecting mild traumatic brain injury from magnetoencephalography data. *PLOS Comput. Biol.* **19**, e1011613 (2023).
- [49] Gramfort, A. *et al.* MEG and EEG data analysis with MNE-Python. *Front. neurosci.* (2013).
- [50] Gramfort, A. *et al.* MNE software for processing MEG and EEG data. *NeuroImage* **86**, 446–460 (2014).
- [51] Taulu, S. & Simola, J. Spatiotemporal signal space separation method for rejecting nearby interference in MEG measurements. *Phys. Med. Biol.* **51**, 1759 (2006).
- [52] Hyvärinen, A. Fast and robust fixed-point algorithms for independent component analysis. *IEEE Trans. Neural Netw.* **10**, 626–634 (1999).
- [53] Dammers, J. *et al.* Integration of amplitude and phase statistics for complete artifact removal in independent components of neuromagnetic recordings. *IEEE Trans Biomed Eng* **55**, 2353–2362 (2008).
- [54] Dale, A. M., Fischl, B. & Sereno, M. I. Cortical surface-based analysis I: Segmentation and surface reconstruction. *NeuroImage* **9**, 179–194 (1999).
- [55] Fischl, B., Sereno, M. I. & Dale, A. M. Cortical surface-based analysis II: Inflation, flattening, and a surface-based coordinate system. *NeuroImage* **9**, 195–207 (1999).
- [56] Ségonne, F. *et al.* A hybrid approach to the skull stripping problem in MRI. *NeuroImage* **22**, 1060–1075 (2004).
- [57] Bardouille, T. & Bailey, L. Evidence for age-related changes in sensorimotor neuromagnetic responses during cued button pressing in a large open-access dataset. *NeuroImage* **193**, 25–34 (2019).
- [58] Dale, A. M. *et al.* Dynamic statistical parametric mapping: Combining fMRI and MEG for high-resolution imaging of cortical activity. *Neuron* **26**, 55–67 (2000).
- [59] Lin, F.-H. *et al.* Assessing and improving the spatial accuracy in MEG source localization by depth-weighted minimum-norm estimates. *NeuroImage* **31**, 160–171 (2006).

- 473 [60] Khan, S. *et al.* Maturation trajectories of cortical resting-state networks depend on the mediating frequency band. *NeuroImage*
474 **174**, 57–68 (2018).
- 475 [61] Desikan, R. S. *et al.* An automated labeling system for subdividing the human cerebral cortex on MRI scans into gyral based
476 regions of interest. *NeuroImage* **31**, 968–980 (2006).
- 477 [62] Fries, P. A mechanism for cognitive dynamics: neuronal communication through neuronal coherence. *Trends Cogn. Sci.* **9**,
478 474–480 (2005).
- 479 [63] Womelsdorf, T. *et al.* Modulation of neuronal interactions through neuronal synchronization. *Science* **316**, 1609–1612 (2007).
- 480 [64] Benjamini, Y. & Hochberg, Y. Controlling the false discovery rate: A practical and powerful approach to multiple testing. *J. R.
481 Stat.* **57**, 289–300 (1995).

482 Acknowledgements

483 Data collection and sharing for this project were provided by the Cambridge Center for Ageing and Neuroscience (Cam-CAN). Cam-
484 CAN funding was provided by the UK Biotechnology and Biological Sciences Research Council (grant number BB/H008217/1),
485 together with support from the UK Medical Research Council and University of Cambridge, UK. S.R. and L.P. disclose support
486 for the research of this work by the National Institute for Neurological Disorders and Stroke (grant number R01NS104585), and
487 the Helsinki–Uusimaa Regional Council. J.C.A.-D. and L.P. disclose support for the research of this work by Business Finland
488 (grant “DIGIMIND” 7981/31/2022) and the Norman Loveless Memorial Fund. M.L. discloses support for the research of this work
489 by the Swedish Cultural Foundation in Finland. We thank Matti S. Hämäläinen for providing comments on the manuscript and
490 acknowledge the computational resources provided by the Aalto Science-IT project.

491 Author contributions

492 S.R., M.L., and L.P. conceived and designed the study. J.C.A.-D. contributed to the methods. S.R. performed investigation and
493 wrote the manuscript. All authors edited the manuscript. L.P. supervised the work.

494 Ethics statement

495 The primary study responsible for data collection was conducted in accordance with the Declaration of Helsinki and was approved
496 by the Cambridgeshire 2 Research Ethics Committee (reference: 10/H0308/50). The participants gave written informed consent for
497 the study. These data were shared with the authors by the Cambridge Center for Ageing and Neuroscience (Cam-CAN) and were
498 handled in accordance with the Cam-CAN data use agreement.

499 Competing interests

500 The authors declare the following competing interests: L.P. has a part-time employment with the MEG device vendor MEGIN Oy.
501 The other authors declare no competing interests.

502 Materials & Correspondence

503 Requests should be addressed to the corresponding author.